How accurately can the deuterium abundance be determined ?

Sergei A. Levshakov[1], Wilhelm H. Kegel[2] and Fumio Takahara[3]

[1]*Department of Theoretical Astrophysics, A. F. Ioffe Physico-Technical Institute, 194021 St. Petersburg, Russia*
[2]*Institut für Theoretische Physik der Universität Frankfurt am Main, Postfach 11 19 32, 60054 Frankfurt/Main, Germany*
[3]*Department of Physics, Tokyo Metropolitan University, Hachioji, Tokyo 192-03, Japan*

Modern observations of the H+D absorption at high redshift play an important role in determining the primordial hydrogen isotopic ratio D/H $\equiv N_{\rm DI}/N_{\rm HI}$ (the ratio of the DI to HI column densities). Measurements of $N_{\rm DI}$ and $N_{\rm HI}$ from QSO spectra can provide a sensitive test of the predictions of big bang nucleosynthesis [BBN] if their precision is comparable with the theoretical uncertainties ($\simeq 15$ %).

It has been shown, however, that the determination of N depends on the assumptions made with respect to the line broadening mechanism and may be ambiguous especially for the case of optically thick lines [1–8]. The commonly used procedure is to fit Voigt profiles, accounting for radiative damping and Doppler broadening in the *microturbulent* limit (completely uncorrelated bulk motions). But the interpretation of observed profiles may be substantially changed if a *mesoturbulent* model is used, i.e. if the influence of a *finite* correlation length in the stochastic velocity field on the line forming process is accounted for. This appears to be appropriate in particular with respect to the H+D absorption observed in QSO spectra. The hydrogen absorbers with $N_{\rm HI} \sim 10^{17} - 10^{18}$ cm^{-2} (which are especially useful for deuterium observations) are usually associated with extended gas halos of foreground galaxies. Direct observations [9] of distant galaxies ($z > 2$) reveal complex morphologies and kinematics of the extended HI Lyα absorption gas with projected sizes up to ~ 50 kpc. The inferred high values of the rms velocity dispersion ($\sigma_t \sim 20 - 50$ km s^{-1}) and a few kpc sizes of the absorbing regions make the mesoturbulent approach more adequate in this case.

Within the framework of the mesoturbulent model, one has to determine both the physical parameters of the gas and the velocity field structure $v(s)$ along the line of sight. This problem may be successfully solved by using a Reverse Monte Carlo [RMC] technique [8].

We applied the RMC procedure to a template H+D Lyα profile which reproduces the Q1009+2956 spectrum with the DI Lyα line seen at $z_a = 2.504$ [10]. Here we present only a part of our results, the full analysis is given in [8].

To simulate real data, we added the experimental uncertainties to the template intensities which were sampled in equidistant bins as shown in Fig. 1 by dots and corresponding error bars. A *one*-component mesoturbulent model with a *homogeneous* density and temperature was adopted. Adequate profile fits for three different sets of parameters are shown in panels (**a1**, **b1**, **c1**) by solid curves, whereas the individual HI and DI profiles are the dashed and dotted curves, respectively. The estimated parameters (D/H, $N_{\rm HI}$, T_{kin}, the ratio of the rms turbulent velocity to the thermal velocity σ_t/v_{th}, the ratio of the cloud thickness to the correlation length L/l) and χ^2_{min} values per degree of freedom are also listed in these panels for each RMC solution.

The essential difference between the results of the *two*-component microturbulent model adopted in [10] and ours lies in the estimation of the hydrodynamical velocities in the $z_a = 2.504$ absorbing region. The RMC procedure yields $\sigma_t \simeq 25$ km s^{-1}, whereas the *two*-component model leads to $\sigma_t \simeq 2$ km s^{-1} which is evidently too low as compared with observations [9].

In this particular absorption system, the study of the H+D Lyα profile yields D/H $= (3.75 \pm 0.85) \times 10^{-5}$ (2σ) which is slightly higher than the value $2.51^{+0.96}_{-0.69} \times 10^{-5}$ found in [10]. This difference is, however, very significant because it leads to limits on D/H consistent with BBN predictions and observational constraints on both extra-galactic ^{4}He mass fraction Y_p [11] and ^{7}Li abundance in the atmospheres of population II (halo) stars [12]. BBN restricts the common interval of the baryon to photon ratio η for which there is concordance between the above-mentioned abundances to $(3.9 - 5.3) \times 10^{-10}$ as shown by the shaded region in Fig. 2. It implies that $0.014 \lesssim \Omega_b h^2_{100} \lesssim 0.020$.

We conclude that the discordance of D/H with the ^{4}He and ^{7}Li measurements noted in [10] is a consequence of the use of the microturbulent model. The generalized mesoturbulent model gives good agreement between the light element abundances and the BBN predictions.

Acknowledgements. This work was supported in part by the RFBR grant No. 96-02-16905-a and by the Deutsche Forschungsgemeinschaft.

References

[1] Levshakov S. A., Kegel W. H., 1994, MNRAS , 271, 161
[2] Levshakov S. A., 1995, Space Sci. Rev., 74, 285
[3] Levshakov S. A., Kegel W. H., 1996, MNRAS , 278, 497
[4] Levshakov S. A., Takahara F., 1996, MNRAS , 279, 651
[5] Levshakov S. A., Takahara F., 1996, Astron. Lett., 22, 491
[6] Levshakov S. A., Kegel W. H., 1997, MNRAS , 288, 787
[7] Levshakov S. A., Kegel W. H., Mazets I. E., 1997, MNRAS , 288, 802
[8] Levshakov S. A., Kegel W. H., Takahara F., 1997, MNRAS , (submit.)
[9] van Ojil R. et al. , 1997, A&A , 317, 358
[10] Burles S., Tytler D., 1996, preprint astro-ph/9603070
[11] Izotov Yu., Thuan T. X., Lipovetsky V. A., 1997, ApJS, 108, 1
[12] Bonifacio P., Molaro P., 1997, MNRAS , 285, 847
[13] Sarkar S., 1996, Rep. Prog. Phys., 59, 1493

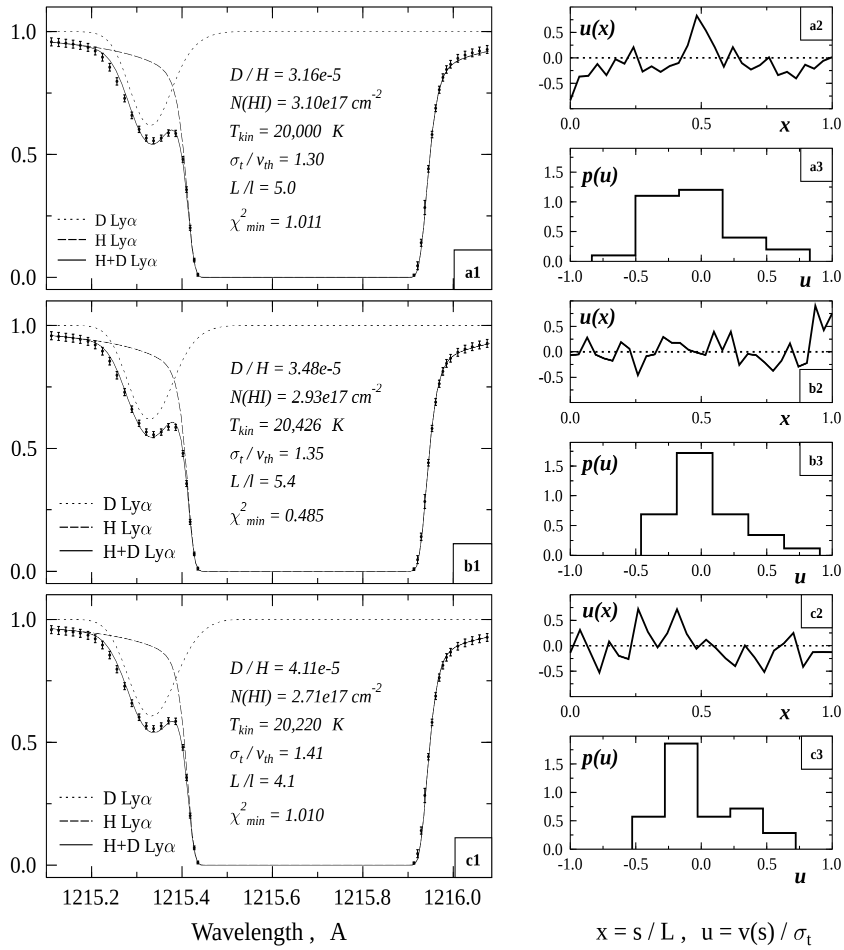

Figure 1: (**a1**, **b1**, **c1**) – A template H+D Lyα profile (dots with error bars) representing the normalized intensities and their uncertainties in accord with [10]. The solid curves show the results of the RMC minimization, whereas the dotted and dashed curves are the separate profiles of DI and HI, respectively. Also shown are the best fitting parameters and the χ^2 values obtained for each case. (**a2**, **b2**, **c2**) – The corresponding individual realizations of the velocity distribution $u(x)$ in units of σ_t. (**a3**, **b3**, **c3**) – The histograms are the projected velocity distributions $p(u)$.

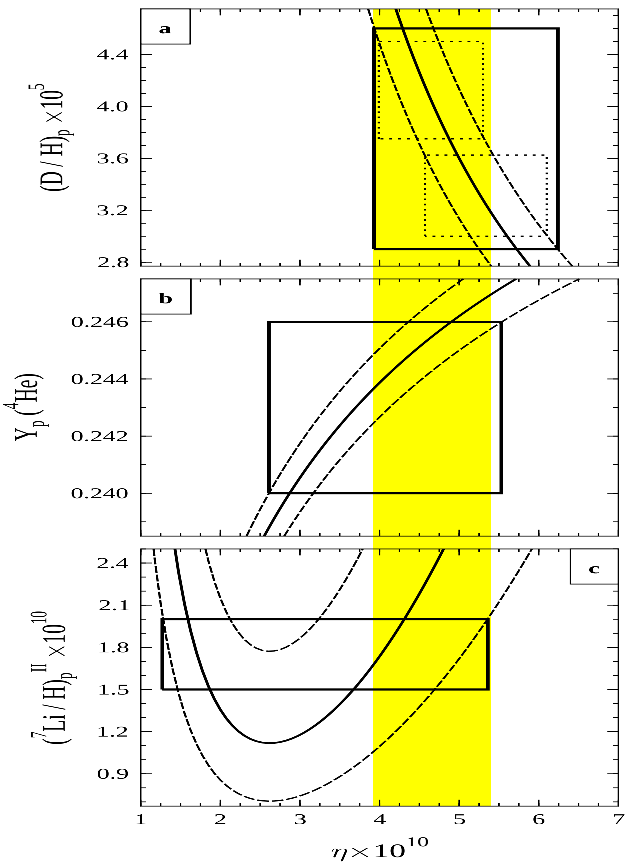

Figure 2: Comparison of predicted primordial abundances (denoted by the subscript p) with observational bounds. The theoretical BBN D, ^{4}He, and ^{7}Li yields (solid curves) and their uncertainties (dashed curves) as function of η (the baryon to photon number ratio) are computed by using the parameterization given in [13]. The abundances of D and ^{7}Li are number ratios, whereas Y_p is the mass fraction of ^{4}He. The hight of the solid-line rectangles in panels **b** and **c** give the bounds from recent measurements of extra-galactic Y_p [11] and ^{7}Li in population II (halo) stars [12]. The horizontal widths give the range of η compatible with the measurements. In panel **a** the solid-line rectangle corresponds to the uncertainty region for D/H towards Q1009+2956, as calculated by the RMC procedure for an arbitrary velocity field configuration [8]. The upper and lower dotted-line rectangles are defined by the confidence regions (computed in [8]) for the fixed velocity field structures shown in Fig. 1(**c2**) and Fig. 1(**a2**), respectively. The shaded region is the window for η common to all results.